

## Activation thick target yield measurement of $^{100}\text{Mo}(\alpha, n)^{103}\text{Ru}$ for studying the weak $r$ -process nucleosynthesis

T. N. Szegedi,<sup>1,2</sup> G. G. Kiss,<sup>2,\*</sup> P. Mohr<sup>2</sup>, A. Psaltis<sup>3</sup>, M. Jacobi<sup>3</sup>,  
G. G. Barnaföldi,<sup>4</sup> T. Szücs<sup>2</sup>, Gy. Gyürky<sup>2</sup> and A. Arcones<sup>3,5</sup>

<sup>1</sup>University of Debrecen, H-4001 Debrecen, Hungary

<sup>2</sup>Institute for Nuclear Research (Atomki), PO Box 51, H-4001 Debrecen, Hungary

<sup>3</sup>Institut für Kernphysik, Technische Universität Darmstadt, Schlossgarten Straße 2, D-64289 Darmstadt, Germany

<sup>4</sup>Wigner Research Centre for Physics, 29-33 Konkoly-Thege Miklós Street, H-1121 Budapest, Hungary

<sup>5</sup>GSI Helmholtzzentrum für Schwerionenforschung GmbH, Planck Straße 1, D-64291 Darmstadt, Germany



(Received 14 May 2021; revised 7 July 2021; accepted 31 August 2021; published 13 September 2021)

**Background:** Light ( $30 \leq Z \leq 45$ ) neutron-rich isotopes are thought to be synthesized in the neutrino-driven ejecta of core-collapse supernovae explosions via the weak  $r$  process. Recent nucleosynthesis studies have demonstrated that  $(\alpha, xn)$  reactions play a particularly important role in the production of these isotopes.  $\alpha$ -nucleus optical model potentials ( $\alpha$ -OMPs) are used to model this nucleosynthesis scenario.

**Purpose:** The different  $\alpha$ -OMP model parameters can affect the calculated cross sections by more than an order of magnitude in the relevant energy regions, which affects the production of light neutron-rich isotopes. Consequently, to constrain the astrophysical conditions characterizing the supernovae ejecta, the uncertainty of the nuclear physics input has to be reduced.

**Methods:** The cross section of the  $^{100}\text{Mo}(\alpha, n)^{103}\text{Ru}$  reaction was measured by means of the activation method. 0.5 mm thick molybdenum disks were irradiated with  $E_\alpha = 7.0$  to  $E_\alpha = 13.0$  MeV  $\alpha$  beams. Thick target yields and reaction cross sections were determined via  $\gamma$ -ray spectroscopy.

**Results:** Cross sections at several energies below the Coulomb barrier were measured, reaching the astrophysically relevant energy region. Large discrepancies between the experimental values and statistical model predictions calculated using the well-known  $\alpha$ -OMPs were found. The measured cross section data could be excellently described by the Atomki-V2 potential. Therefore, this  $\alpha$ -OMP was used to derive the astrophysical reaction rates as a function of temperature.

**Conclusions:** The successful reproduction of the measured cross sections in a wide energy region confirm the reliability of the Atomki-V2 potential. The usage of the new  $^{100}\text{Mo}(\alpha, n)^{103}\text{Ru}$  experimental data along with the Atomki-V2 potential reduces the nuclear uncertainties of the weak  $r$ -process production yields of nuclei with  $36 \leq Z \leq 50$  to a marginal level.

DOI: [10.1103/PhysRevC.104.035804](https://doi.org/10.1103/PhysRevC.104.035804)

### I. INTRODUCTION

The bulk of the stable isotopes heavier than iron are formed via neutron capture reactions in the so-called  $s$  and  $r$  processes [1,2]. However, in order to properly reproduce the observed amount of heavy isotopes, the contribution from further nucleosynthesis processes has to be taken into account. Indeed, low mass neutron-rich isotopes, located between iron and silver, may be formed by neutron captures combined with  $(\alpha, xn)$  and  $(p, xn)$  reactions in the neutrino-driven ejecta from core-collapse supernovae explosions [3–6]. The matter which is ejected contains mainly protons, neutrons, and  $\alpha$  particles, since it is close to the nascent neutron star. Initially, the abundances remain in nuclear statistical equilibrium due to the high temperature [7], but, as matter expands, the temperature and the density decrease and protons and  $\alpha$  particles start to build

up heavier nuclei by, e.g.,  $(\alpha, xn)$  and  $(p, xn)$  reactions [8–10]. This is the basic picture of the weak  $r$  process (also referred to as the  $\alpha$  process [3]).

The modeling of this nucleosynthesis scenario requires the use of an extended reaction network involving a few thousand, mostly unstable nuclei. The necessary reaction rates are calculated from the cross sections computed with the Hauser-Feshbach statistical model which relies on different nuclear physics ingredients [11]. Series of sensitivity calculations were performed to study the impact of the calculated cross sections on the nucleosynthesis yields and the related uncertainty of the models [10,12]. It was found that the main source of the uncertainty arises from the choice of different  $\alpha$ -nucleus optical model potential ( $\alpha$ -OMP) parameter sets. Namely, the difference between the cross sections calculated using different  $\alpha$ -OMPs can exceed even one order of magnitude at the energies of interest [8–10]. Unfortunately, there is a lack of high-precision experimental data reaching the astrophysically relevant energies necessary to assess the

\*gkiss@atomki.hu

cross section predictions calculated using different  $\alpha$ -OMP. Without such data, the nuclear physics input of the weak  $r$ -process nucleosynthesis calculations remains uncertain which prevents the understanding of the astrophysical environment of the process.

Even if the  $^{100}\text{Mo}(\alpha, n)^{103}\text{Ru}$  reaction was not identified as highly critical by Bliss *et al.*, this is one of the few reactions in the relevant mass region where cross section measurements at astrophysical energies are technically feasible. Accordingly, to improve our knowledge on the  $\alpha$ -OMPs used in the weak  $r$ -process nucleosynthesis calculations, this reaction was studied in the present work using the thick target yield (TTY) method. In most of the activation cross section measurements thin targets are used; i.e., the energy loss of the projectile in the target is small. In such cases the reaction cross section can be derived at an effective energy slightly below the beam energy if the target thickness is known. Alternatively, in the present work the TTY was measured. The advantage of this approach is that the projectile stops completely in the target and thus the number of target atoms is maximized. According to this, reactions take place with all energies between the bombarding energy and the reaction threshold. Thus, experimentally the number of reactions per projectile is measured. The cross sections are then derived from the difference of the TTYs at two neighboring energies.

This paper is organized as follows. Details on the experimental technique are presented in Sec. II. The resulted astrophysical  $S$  factors<sup>1</sup> are presented and compared with predictions calculated using well-known  $\alpha$ -OMPs in Sec. III. Finally, in Sec. IV the astrophysical reaction rates calculated from the measured thick target yields are listed and conclusions are drawn.

## II. EXPERIMENTAL APPROACH

The experiment was carried out at the Institute for Nuclear Research (Atomki) using the activation technique [14]. Molybdenum ( $Z = 42$ ) has seven stable isotopes from  $^{92}\text{Mo}$  to  $^{100}\text{Mo}$ .  $\alpha$ -induced reactions on molybdenum lead to different ruthenium isotopes including radioactive ones. Using the activation method, it is feasible to derive the cross sections of the  $^{92}\text{Mo}(\alpha, n)^{95}\text{Ru}$ ,  $^{94}\text{Mo}(\alpha, n)^{97}\text{Ru}$ , and  $^{100}\text{Mo}(\alpha, n)^{103}\text{Ru}$  reactions. In this work, we report on the  $^{100}\text{Mo}(\alpha, n)^{103}\text{Ru}$  reaction cross section measurement. The results from the former two reactions will be published elsewhere [15]. The produced  $^{103}\text{Ru}$  isotope has a half-life of  $T_{1/2} = 39.247 \pm 0.013$  d and its  $\beta^-$  decay is followed by the emission of  $E_\gamma = 497.09$  keV ( $I_\gamma = 91.0 \pm 1.2\%$ ) and  $E_\gamma = 610.33$  keV ( $I_\gamma = 5.76 \pm 0.06\%$ )  $\gamma$  rays [16]. However, the latter  $\gamma$  transition is located close—within the resolution of the high-purity germanium (HPGe) detectors used for the activity measurements—to the  $E_\gamma = 609.32$  keV background line originating from the decay of  $^{214}\text{Bi}$ . Therefore, the weaker transition was not used for the determination of the thick target yield.

The thickness of the natural isotopic composition molybdenum plates, irradiated with  $\alpha$  beams provided by the  $K = 20$  cyclotron accelerator of Atomki, was 0.5 mm. The energy of the  $\alpha$  beam was between  $E_{\text{lab}} = 7.0$  MeV and  $E_{\text{lab}} = 13.0$  MeV, and this energy range was scanned with energy steps of 0.3–1.0 MeV. Thus, the projectile stops in the target and reactions take place with all energies between the bombarding energy and the reaction threshold. Accordingly, the measured thick target yield  $Y_{TT}(E)$  as a function of  $\alpha$  energy ( $E$ ) is related to the integrated reaction cross section  $\sigma(E)$  [17]:

$$Y_{TT}(E) = \int_{E_{\text{thr}}}^E \frac{\sigma(E')}{\epsilon_{\text{eff}}(E')} dE', \quad (1)$$

where  $E_{\text{thr}} = 4.76$  MeV is the reaction threshold in the laboratory system and  $\epsilon_{\text{eff}}(E)$  is the effective stopping power for the  $^{100}\text{Mo}$  nucleus.<sup>2</sup> From the measured  $Y_{TT}(E)$  data, the cross section between two neighboring energies, can be obtained by subtraction:

$$\sigma(E_{\text{eff}}) = \frac{[Y_{TT}(E_2) - Y_{TT}(E_1)]\overline{\epsilon_{\text{eff}}}(E_2; E_1)}{E_2 - E_1}, \quad (2)$$

where  $\overline{\epsilon_{\text{eff}}}(E_2; E_1)$  is the averaged effective stopping power corresponding to the energy of two neighboring irradiations.

The length of the irradiations varied between  $t_{\text{irrad.}} = 0.5$  h and  $t_{\text{irrad.}} = 48.28$  h with beam currents of 0.4–1.6  $\mu\text{A}$ . The number of the impinging  $\alpha$  particles was determined from current measurement. After the beam-defining aperture, the chamber was insulated and served as a Faraday cup. Furthermore, a secondary electron suppression voltage of  $-300$  V was applied at the entrance of the chamber. The collected charge was measured with a current integrator. The integrator counts were recorded using multichannel scaling mode to take into account small fluctuations of the beam current.

The activity of the irradiated samples was measured using 50% (detA) and a 100% (detB) relative efficiency HPGe detectors, both equipped with lead shielding. The  $\gamma$  counting was carried out in two geometries. The activity of the sources irradiated with  $\alpha$  beams of  $E_{\text{lab}} = 10$  MeV and above were measured at the so-called far geometry [i.e., the targets were placed 21 cm (detA) and 27 cm (detB) away from the detector end cap]. However, the low yields necessitated the use of short [5 cm (detA) and 1 cm (detB)] source-to-detector distances for the targets, irradiated with alpha beams of  $E_{\text{lab}} = 9.5$  MeV and below.

The absolute detection efficiencies were measured solely in far geometry using calibrated  $^{60}\text{Co}$ ,  $^{133}\text{Ba}$ ,  $^{137}\text{Cs}$ ,  $^{152}\text{Eu}$ , and  $^{241}\text{Am}$  sources. The calibration sources emit multiple  $\gamma$  rays from cascade transitions. Thus, due to the so-called true-coincidence summing effect [18], in short source-to-detector distances no direct efficiency measurement was carried out. Instead, the activity of the targets irradiated with  $\alpha$  beams of  $E_\alpha = 11.5$  MeV and at  $E_\alpha = 13.0$  MeV were measured in both close and far geometry. Taking into account the time

<sup>1</sup>The astrophysical  $S$  factors are calculated from the measured cross sections using the equation [13]  $S(E) \equiv E e^{(2\pi\eta)} \sigma(E)$ .

<sup>2</sup>The stopping power, given in  $\text{eV}/(\text{atom}/\text{cm}^2)$ , of chemically pure molybdenum was divided by the abundance of  $^{100}\text{Mo}$  ( $9.81 \pm 0.31\%$ ).

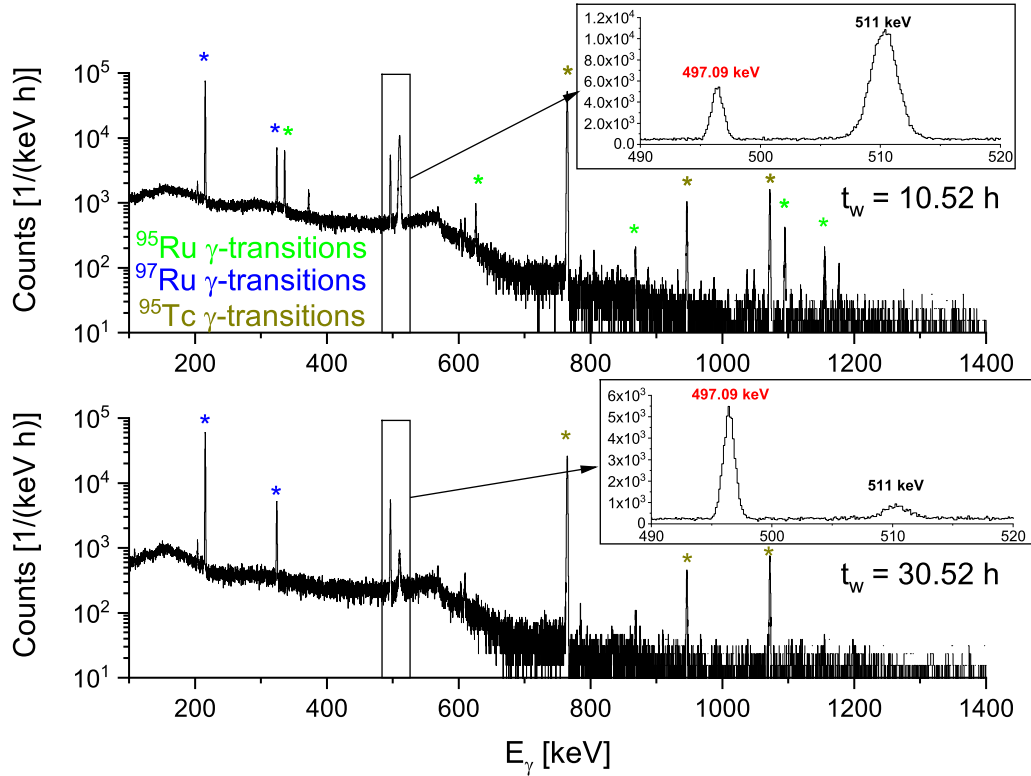


FIG. 1. Offline  $\gamma$ -ray spectra taken  $t_w = 10.52$  h (top) and  $t_w = 30.52$  h (bottom) after irradiating a molybdenum target with an  $E_\alpha = 11.0$  MeV beam. The  $\gamma$  peak used to derive the cross sections is shown in the insets on linear scale. The  $E_\gamma = 511$  keV background peak and transitions corresponding to  $\alpha$ -induced reactions on other molybdenum isotopes are marked with stars.

elapsed between the two countings, a conversion factor of the efficiencies between the two geometries was determined and henceforward used in the analysis. The conversion factors determined from the  $E_\alpha = 11.5$  MeV and at  $E_\alpha = 13.0$  MeV countings were found to be in agreement within their statistical uncertainties. The above described procedure automatically accounts also for true-coincidence summing in the decay of  $^{103}\text{Ru}$ . Accordingly, the detection efficiency in far geometry for measuring an  $E_\gamma = 497.07$  keV  $\gamma$  ray was found to be 0.156% ( $\pm 3.5\%$ ) and the weighted mean of the far-to-close geometry conversion factors is 7.87 ( $\pm 0.17\%$ ).

After the irradiations,  $t_w \approx 2.0$  h waiting time was used in order to let the short-lived, unwanted activities decay. The duration of the  $\gamma$  countings was typically 5–21 days and the spectra were saved every hour. Typical offline  $\gamma$  spectra are presented in Fig. 1. To enhance the signal-to-noise ratio, the two lowest energy data points were measured using detA at the Jánossy Underground Research Laboratory located at the Wigner Research Centre for Physics (Budapest, Hungary). The laboratory background count rate within the peak width at the  $E_\gamma = 497.09$  keV transition at this site is about a factor of 4 lower than at Atomki (about 0.15/keV s at Atomki and 0.04/keV s at Wigner RCP, respectively). The peaks were fitted with a Gaussian function with a linear background. The detected counts ( $C$ ) are related to the counting and irradiation parameters as follows:

$$C = Y_{TT} \eta I_\gamma \sum_{i=1}^n (\phi_i e^{-(n-i)\lambda\Delta t}) \frac{e^{-\lambda t_w} (1 - e^{-\lambda t_c})}{\lambda}, \quad (3)$$

where  $\eta$  is the absolute detection efficiency,  $I_\gamma$  is the branching ratio of the 497.09 keV transition,  $\phi$  is the number of the incident  $\alpha$  particles in the  $i$ th one-minute time window ( $\Delta t$ ) of the multichannel scaler,  $\lambda$  is the decay constant, and  $n\Delta t$ ,  $t_w$ ,  $t_c$  are the length of the irradiation, the waiting time between the end of the irradiation and the beginning of the countings, and the duration of the counting, respectively. Since thick targets were used and accordingly the created activity is distributed in the bulk of the target, the attenuation of the emitted  $\gamma$  radiation has to be taken into account. A similar procedure, described in detail in Ref. [19], was used to determine the activity distribution in the molybdenum plate and the corresponding attenuation factors. Namely, we assumed that the target is built up from 0.01  $\mu\text{m}$  thick uniform layers. The estimated activity distribution was then weighted by the attenuation factor corresponding to each layer. It was found that the bulk of the activity is created in the first few  $\mu\text{m}$ ; the attenuation corresponding to the  $E_\gamma = 497.09$  keV  $\gamma$  ray at these depths is below 0.1%. According to this, the total loss due to the  $\gamma$ -ray attenuation is less than 0.15%, which is negligible.

### III. RESULTS AND THEORETICAL ANALYSIS

The measured  $^{100}\text{Mo}(\alpha, n)^{103}\text{Ru}$  thick target yields are listed in Table I. The activity of several irradiated targets was measured with both detA and detB detectors and always consistent yields were found. In Table I the average values, weighted by the statistical uncertainties are listed. The listed TTY uncertainties were derived as the quadratic sum

TABLE I. Thick target yield and cross section of the  $^{100}\text{Mo}(\alpha, n)^{103}\text{Ru}$  reaction.

$E_{c.m.}$ (MeV)	Thick target yield (reaction/projectile)	$E_{\text{eff};c.m.}$ (MeV)	$\sigma$ (barn)
12.50	$(4.58 \pm 0.04) \times 10^{-7}$	$12.14 \pm 0.05$	$(8.49 \pm 0.69) \times 10^{-2}$
11.78	$(2.77 \pm 0.07) \times 10^{-7}$	$11.66 \pm 0.05$	$(9.09 \pm 0.75) \times 10^{-2}$
11.54	$(2.14 \pm 0.03) \times 10^{-7}$	$11.32 \pm 0.05$	$(8.46 \pm 0.67) \times 10^{-2}$
11.06	$(9.90 \pm 0.14) \times 10^{-8}$	$10.85 \pm 0.05$	$(4.02 \pm 0.32) \times 10^{-2}$
10.58	$(4.58 \pm 0.06) \times 10^{-8}$	$10.47 \pm 0.05$	$(2.76 \pm 0.25) \times 10^{-2}$
10.34	$(2.79 \pm 0.14) \times 10^{-8}$	$10.23 \pm 0.05$	$(1.58 \pm 0.15) \times 10^{-2}$
10.10	$(1.78 \pm 0.02) \times 10^{-8}$	$9.99 \pm 0.04$	$(1.19 \pm 0.09) \times 10^{-2}$
9.86	$(1.03 \pm 0.02) \times 10^{-8}$	$9.75 \pm 0.04$	$(7.21 \pm 0.59) \times 10^{-3}$
9.61	$(5.82 \pm 0.12) \times 10^{-9}$	$9.44 \pm 0.04$	$(3.32 \pm 0.27) \times 10^{-3}$
9.13	$(1.79 \pm 0.02) \times 10^{-9}$	$9.05 \pm 0.04$	$(1.49 \pm 0.12) \times 10^{-3}$
8.94	$(1.08 \pm 0.02) \times 10^{-9}$	$8.82 \pm 0.04$	$(8.98 \pm 0.72) \times 10^{-4}$
8.65	$(4.51 \pm 0.07) \times 10^{-10}$	$8.54 \pm 0.04$	$(3.70 \pm 0.31) \times 10^{-4}$
8.36	$(1.97 \pm 0.06) \times 10^{-10}$	$8.23 \pm 0.04$	$(1.51 \pm 0.13) \times 10^{-4}$
7.98	$(6.14 \pm 0.16) \times 10^{-11}$	$7.85 \pm 0.03$	$(5.23 \pm 0.48) \times 10^{-5}$
7.60	$(1.58 \pm 0.07) \times 10^{-11}$	$7.49 \pm 0.03$	$(1.70 \pm 0.21) \times 10^{-5}$
7.31	$(4.98 \pm 0.43) \times 10^{-12}$	$7.20 \pm 0.03$	$(5.70 \pm 0.76) \times 10^{-6}$
7.02	$(1.45 \pm 0.10) \times 10^{-12}$	$6.91 \pm 0.03$	$(1.62 \pm 0.20) \times 10^{-6}$
6.73	$(4.70 \pm 0.32) \times 10^{-13}$		

of the statistical uncertainties ( $\leq 8.6\%$ ), the uncertainty of the branching ratio (1.3%), the uncertainty of the detection efficiency (3.5%), and the beam current uncertainty (3%).

The effective interaction energy ( $E_{\text{eff}}$ ) is determined from the yield curve:

$$Y_{TT}(E_{\text{eff}}) = \frac{[Y_{TT}(E_2) - Y_{TT}(E_1)]}{2}. \quad (4)$$

An exponential curve was fitted to the measured TTY points;  $E_{\text{eff}}$  is defined where the integrals of the exponential in the  $E_1$ - $E_{\text{eff}}$  and  $E_{\text{eff}}$ - $E_2$  regions are equal. The quoted effective energy was calculated by Eq. (4) from this fitted curve; the quoted uncertainty corresponds to the energy calibration of the  $\alpha$  beam and to the uncertainty of the energy loss in the target, which was calculated using the SRIM code [20]. The average cross section between two energies was derived from the thick target yield using Eq. (2). The astrophysically

relevant energy region (Gamow window) ranges from  $E_{\text{min}} = 4.8$  MeV up to  $E_{\text{max}} = 6.5$  MeV at  $T = 2$  GK temperature, from  $E_{\text{min}} = 5.9$  MeV up to  $E_{\text{max}} = 8.4$  MeV at  $T = 3$  GK, and from  $E_{\text{min}} = 6.9$  MeV up to  $E_{\text{max}} = 9.9$  MeV at  $T = 4$  GK. An explanation of the Gamow window will be given later at the beginning of Sec. IV. The derived astrophysical  $S$  factors are shown in Fig. 2 in comparison with theoretical predictions calculated using different global  $\alpha$ -OMPs.

The  $^{100}\text{Mo}(\alpha, n)^{103}\text{Ru}$  reaction was already studied in the 1960s and 1970s by Esterlund *et al.* [21] and Graf *et al.* [22]. For comparison, the data from literature [21,22] are shown on the left side in Fig. 2. The energy dependence of the literature data is clearly different: at higher energies (above  $E_{c.m.} = 15$  MeV) the data of Graf exceed the cross sections measured by Esterlund by about 50%. In contrast, at energies below  $E_{c.m.} = 15$  MeV the Esterlund *et al.* data are significantly higher. Since the two data sets are contradictory, the theoretical analysis is restricted to our new experimental results.

The theoretical analysis follows closely our previous work on the  $^{96}\text{Zr}(\alpha, n)^{99}\text{Mo}$  reaction [23]. In a schematic notation, the cross section in the statistical model (SM) for an  $\alpha$ -induced reaction of  $(\alpha, X)$  type is given by

$$\sigma(\alpha, X) \sim \frac{T_{\alpha,0} T_X}{\sum_i T_i} = T_{\alpha,0} \times b_X \quad (5)$$

with the transmission coefficients  $T_{\alpha,0}$  of the incoming  $\alpha$  particle,  $T_i$  for the outgoing particles ( $i = \gamma, p, n, \alpha, 2n$ , etc.), and the branching ratio  $b_X = T_X / \sum_i T_i$  for the branching into the  $X$  channel. Usually, the transmission coefficients  $T_i$  are calculated from optical model potentials for the particle channels and from the  $\gamma$ -ray strength function for the  $(\alpha, \gamma)$  capture channel. For further details, see, e.g., [24,25].

In the energy range under study, the  $(\alpha, n)$  channel dominates, leading to a branching  $b_n$  close to unity for the neutron channel. Only at the highest energy is there a noticeable contribution of the  $(\alpha, 2n)$  reaction. As long as  $b_n \approx 1$  in Eq. (5), the cross section of the  $(\alpha, n)$  reaction essentially depends only on the transmission  $T_{\alpha,0}$  and thus only on the chosen  $\alpha$ -OMP. As a consequence, the relevance of all other ingredients of the SM remains marginal at astrophysically relevant energies. At the highest energy under study, the calculated branching ratios  $b_n$  and  $b_{2n}$  between the  $(\alpha, n)$  and  $(\alpha, 2n)$

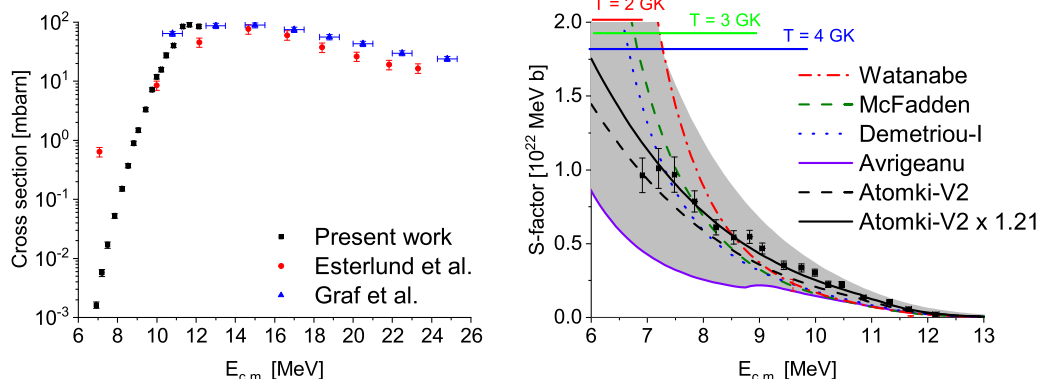


FIG. 2. Experimental cross sections (left), experimental and theoretical astrophysical  $S$  factors (right) as a function of the energy of the  $^{100}\text{Mo}(\alpha, n)^{103}\text{Ru}$  reaction. The colored lines indicate the Gamow windows for the reaction at  $T = 2, 3$ , and 4 GK. For details, see text.

cross sections depends on the chosen level density, leading to a range of predictions for the  $(\alpha, n)$  channel within about  $\pm 20\%$  of the calculation with the default settings.

The following calculations were done by using the present standard TALYS version 1.95 [26] and a modified version of TALYS-V1.8; the latter was used to implement the new Atomki-V2 potential (see below). No significant differences were found between the two versions. This holds also for the earlier version TALYS-V1.6 which was used in previous sensitivity studies (e.g., [8]). The input parameters for TALYS were kept at their standard values in the present study except the  $\alpha$ -OMP, which will be discussed in more detail in the following.

In a first step, the range of predicted  $(\alpha, n)$  cross sections from all eight available options for the  $\alpha$ -OMP was investigated. It is found that the predictions vary by more than one order of magnitude at energies close above the threshold around 5 MeV and by about a factor of 3 around 10 MeV; this range of predictions is shown as the grey-shaded area in Fig. 2. For better readability of Fig. 2, lines are shown only for the following  $\alpha$ -OMPs: the default  $\alpha$ -OMP in previous versions of TALYS by Watanabe [27], the widely used simple four-parameter  $\alpha$ -OMP by McFadden and Satchler [28], one of the  $\alpha$ -OMPs of Demetriou *et al.* [29] (version 1), and the present default  $\alpha$ -OMP by Avrigeanu *et al.* [30]. It is obvious from Fig. 2 that all  $\alpha$ -OMPs have a trend to underestimate the new experimental data at higher energies whereas at the lowest energies most  $\alpha$ -OMPs overestimate the new data.

In addition to the available options for  $\alpha$ -OMPs in TALYS, the new Atomki-V2 potential [31] is used to predict the  $^{100}\text{Mo}(\alpha, n)^{103}\text{Ru}$  cross section. The Atomki-V2 potential is based on elastic scattering data and the barrier transmission approach; for details, see [23,32] and the Supplemental Material of [31]. Similar to the findings in our recent investigation of  $^{96}\text{Zr}(\alpha, n)^{99}\text{Mo}$ , the Atomki-V2 potential reproduces the energy dependence of the new data. A minor adjustment of the absolute scale of the calculated cross sections by a normalization factor of 1.21 leads to an excellent agreement with the experimental data with a  $\chi^2$  per point of about 2.0 and an average deviation of only 10%. Other  $\alpha$ -OMPs require larger normalization factors, but nevertheless do not reach the small  $\chi^2$  of the Atomki-V2 potential; e.g., the second version of the Demetriou potentials reaches a  $\chi^2$  per point of about 3.0 after normalization by a factor of 2.

#### IV. ASTROPHYSICAL RESULTS

The adjusted best fit using the Atomki-V2  $\alpha$ -OMP was used for the calculation of the astrophysical rate for the  $^{100}\text{Mo}(\alpha, n)^{103}\text{Ru}$  reaction (see Table II) using the standard formalism [13]:

$$N_A \langle \sigma v \rangle = N_A \left( \frac{8}{\pi m} \right)^{\frac{1}{2}} \frac{1}{(k_B T)^{3/2}} \int_{E_{\text{thr}}}^{\infty} E \sigma(E) e^{-\frac{E}{k_B T}} dE, \quad (6)$$

where  $N_A$  is the Avogadro number,  $m$  is the reduced mass of the interacting particles,  $\sigma(E)$  is the cross section measured at a given energy  $E$ ,  $E_{\text{thr}}$  is the reaction threshold ( $E_{\text{thr}} = 4.76$  MeV),  $k_B$  is the Boltzmann constant, and  $T$  is the temperature

TABLE II. Recommended astrophysical rate of the  $^{100}\text{Mo}(\alpha, n)^{103}\text{Ru}$  reaction.

$T_9$	$N_A \langle \sigma v \rangle$ ( $\text{cm}^3 \text{s}^{-1} \text{mole}^{-1}$ )
1.0	$1.04 \times 10^{-24}$
1.5	$1.12 \times 10^{-16}$
2.0	$2.65 \times 10^{-12}$
2.5	$2.40 \times 10^{-9}$
3.0	$4.23 \times 10^{-7}$
4.0	$6.98 \times 10^{-4}$
5.0	$8.11 \times 10^{-2}$

of the environment. The uncertainty of the new rate is estimated to be about 30% for the relevant temperature range (for a discussion of uncertainties, see Ref. [23]).

The astrophysically relevant energies, the so-called effective Gamow window, are derived from the energy dependence of the integrand of Eq. (6). Note that the widely used simple formula for the Gamow window (see, e.g., the textbook of Iliadis [13]) are not applicable in the case of negative  $Q$  values because a constant  $S$  factor is assumed in the standard formula. Instead, the Gamow windows in the present study (as shown in Fig. 2) were calculated from the theoretical energy dependence of the  $S$  factor from the Atomki-V2  $\alpha$ -OMP.

It is worth emphasizing that the  $^{100}\text{Mo}(\alpha, n)^{103}\text{Ru}$  rate exceeds other  $Z \rightarrow Z + 2$  rates for the production of ruthenium from  $^{100}\text{Mo} + \alpha$ , e.g.,  $^{100}\text{Mo}(\alpha, \gamma)^{104}\text{Ru}$  or  $^{100}\text{Mo}(\alpha, 2n)^{102}\text{Ru}$ , by at least one order of magnitude in the relevant temperature range. Accordingly, the role of these other  $Z \rightarrow Z + 2$  reactions remains marginal under typical astrophysical conditions.

The impact of the new  $^{100}\text{Mo}(\alpha, n)^{103}\text{Ru}$  reaction rate on the nucleosynthesis of “light heavy” elements between strontium and silver ( $Z = 38-47$ ) in the neutron-rich neutrino driven ejecta of supernova explosions was studied via extensive nucleosynthesis calculations. We used the same 36 trajectories as in the sensitivity study of Bliss *et al.* [12], which represent typical weak  $r$ -process astrophysical conditions.

For our nucleosynthesis calculations we used the WINNET reaction network code [33]. For the baseline case, the reaction rates were taken from the JINA Reaclib V2.0 database [34,35] with the exception of the  $(\alpha, n)$  reactions, for which we employed the Hauser-Feshbach predictions of TALYS-V1.6 with the default  $\alpha$ -OMP parametrization (referred to as GAOP from here on; for more details see Refs. [8,12,27,36]). The baseline case will be compared to nucleosynthesis calculations using the new recommended rate.

Figure 3 shows the elemental abundances for trajectory MC13 of Ref. [12] using a factors of 3 and 10 uncertainty on the GAOP rate and 30% on the updated new recommended rate. Using the new  $^{100}\text{Mo}(\alpha, n)^{103}\text{Ru}$  reaction rate, we confirm the minor production of elements beyond  $Z \geq 48$  in these conditions. In addition, from the lower panel of Fig. 3 we see a reduction in the uncertainty of palladium, cadmium, indium and tin ( $Z = 46, 48-50$ ) production from up to a factor of 2 to  $\approx 10\%$ . It has to be emphasized that the affected abundances are very small to have any significant effect on the production

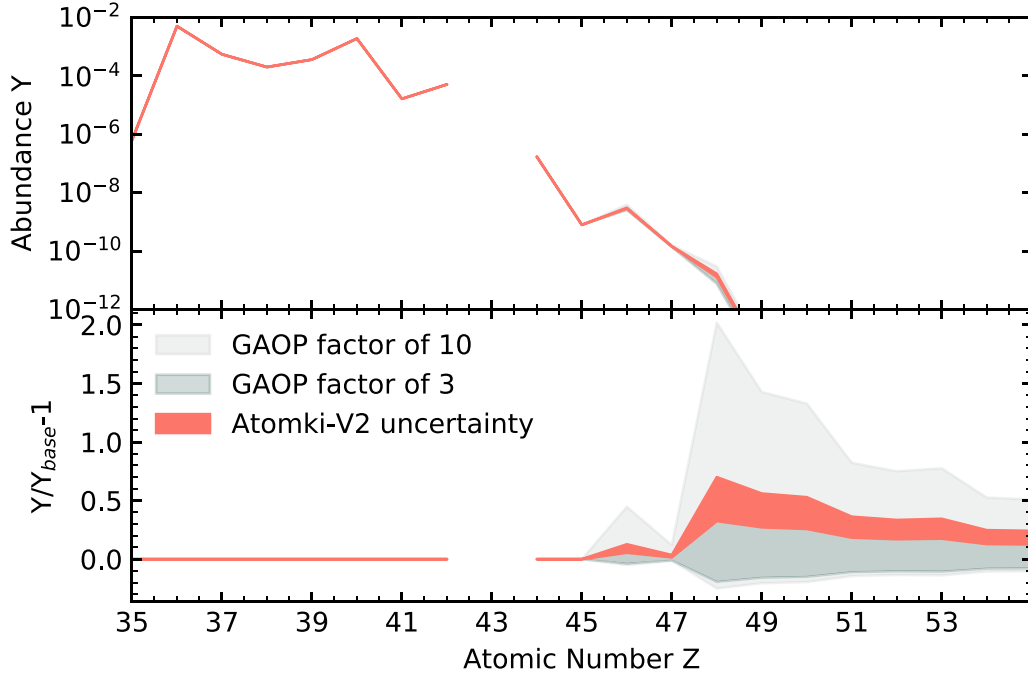


FIG. 3. Elemental abundances for the MC13 trajectory from the study of Ref. [12] (top). The dark and light shaded regions correspond to uncertainty factors of 3 and 10 respectively, while the experimental uncertainty of 30% of the present work is depicted with the colored band. Abundance uncertainties relative to the unvaried GAOP reaction rate ( $Y_{\text{base}}$ ) for the same three different cases (bottom). See the text for details.

of lighter heavy nuclei in the neutrino-driven winds of core-collapse supernovae.

Furthermore, a similar effect on the  $46 \leq Z \leq 50$  abundances was observed in three more trajectories from Ref. [12], namely in MC05, MC15, and MC35. All of these trajectories represent similar astrophysical conditions (see Table I and Fig. 1 in Ref. [12]), with electron fractions  $0.43 < Y_e < 0.48$ , entropy  $48k_B < s < 103k_B$  per nucleon, expansion time  $13 < \tau_{\text{exp}} < 35.9$  ms, neutron-to-seed ratio of  $10^{-4} < Y_n/Y_{\text{seed}} < 10^{-3}$ , and  $\alpha$ -to-seed ratio of  $10 < Y_\alpha/Y_{\text{seed}} < 100$ . The new  $^{100}\text{Mo}(\alpha, n)^{103}\text{Ru}$  reaction rate reduces the production uncertainty of the aforementioned elements to  $\approx 10\%$  under these astrophysical conditions.

## V. SUMMARY AND OUTLOOK

To further investigate the predictive power of the Atomki-V2 potential used for modeling the weak  $r$ -process nucleosynthesis, the  $^{100}\text{Mo}(\alpha, n)^{103}\text{Ru}$  reaction was studied. The reaction cross sections were measured for the first time from energies slightly above the reaction threshold up to  $E_{c.m.} = 12.5$  MeV using the thick target yield method. The new high-precision data have been analyzed in the statistical model. It was found that the calculation performed using the new Atomki-V2 potential, rescaled by 1.21, excellently describes the new experimental data while the other  $\alpha$ -OMP cannot reproduce the energy dependence of the measured cross sections with the same accuracy. The scaled Atomki-V2 calculation was then used to derive the astrophysical reaction rates as a function of temperature. For the full temperature range of the weak  $r$  process, the uncertainty of the reaction rate could

be drastically reduced from the usually assumed factor of 10 down to about 30%.

It was found that the  $^{100}\text{Mo}(\alpha, n)^{103}\text{Ru}$  reaction does not significantly affect the production of lighter heavy nuclei via the weak  $r$  process. However, using the new experimental data along with the Atomki-V2 potential, the nuclear uncertainties on the production yields of nuclei with  $36 \leq Z \leq 50$  from the  $^{100}\text{Mo}(\alpha, n)^{103}\text{Ru}$  reaction are now marginal at about 10% or less.

The predictions of the Atomki-V2 potential were found to be reliable within 30% in two experiments carried out for targets around  $A \approx 100$  with partially different techniques and instrumentation. Furthermore, the Atomki-V2 predictions typically do not deviate by more than a factor of 2 from experimental data over a wide mass range. A recalculation of the full weak  $r$ -process network is in progress using the predictions of this potential. The Atomki-V2 potential is derived from the simple and robust approach of barrier transmission, and there are no adjustable parameters. These are prerequisites for reliable extrapolations to unstable nuclei. Sensitivity studies in the Supplemental Material of [31] have shown that predictions from the Atomki-V2 potential should be reliable within a factor of 2 or better also for the mostly unstable target nuclei which are relevant for weak  $r$ -process studies (compared to the usually assumed uncertainty of at least one order of magnitude for  $\alpha$ -induced reaction rates). A verification of this claim can be expected in the near future from upcoming experiments. If the reliability of the Atomki-V2 predictions is verified, this will lead to more robust nucleosynthesis yields and will thus allow to constrain the astrophysical conditions and the site of the weak  $r$  process.

## ACKNOWLEDGMENTS

The authors thank Julia Bliss, Fernando Montes, Jorge Pereira, and Zs. Fülöp for valuable discussions. This work was supported by NKFIH (NN128072, K134197, FK134845) and by the Wigner RCP's Jánossy Underground Research Laboratory infrastructure by the New National Excellence

Program of the Ministry of Human Capacities of Hungary (ÚNKP-20-5-DE-2 and ÚNKP-20-5-DE-297). G.G.K. and T.S. acknowledge support from the János Bolyai research fellowship of the Hungarian Academy of Sciences. A.P., M.J., and A.A. were supported by the ERC Starting Grant EUROPIUM-677912, Deutsche Forschungsgemeinschaft through SFB 1245.

- 
- [1] F. Käppeler, R. Gallino, S. Bisterzo, and W. Aoki, *Rev. Mod. Phys.* **83**, 157 (2011).
- [2] J. J. Cowan, C. Sneden, J. E. Lawen, A. Aprahamian, M. Wiescher, K. Langanke, G. Martinez-Pinedo, and f. K. Thielemann, *Rev. Mod. Phys.* **93**, 015002 (2021).
- [3] B. Meyer *et al.*, *Astrophys. J.* **399**, 656 (1992).
- [4] Y. Qian and G. J. Wasserburg, *Phys. Rep.* **442**, 237 (2007).
- [5] A. Arcones and F. Montes, *Astrophys. J.* **731**, 5 (2011).
- [6] A. Arcones and J. Bliss, *J. Phys. G.* **41**, 044005 (2014).
- [7] S. E. Woosley and R. D. Hoffman, *Astrophys. J.* **395**, 202 (1992).
- [8] J. Pereira and F. Montes, *Phys. Rev. C* **93**, 034611 (2016).
- [9] P. Mohr, *Phys. Rev. C* **94**, 035801 (2016).
- [10] J. Bliss, A. Arcones, F. Montes, and J. Pereira, *J. Phys. G* **44**, 054003 (2017).
- [11] W. Hauser and H. Feshbach, *Phys. Rev.* **87**, 366 (1952).
- [12] J. Bliss, A. Arcones, F. Montes, and J. Pereira, *Phys. Rev. C* **101**, 055807 (2020).
- [13] C. Iliadis, *Nuclear Physics of Stars* (Wiley-VCH, Weinheim, 2007).
- [14] G. Gyürky, Z. Fülöp, F. Käppeler, G. G. Kiss, and A. Wallner, *Eur. Phys. J. A* **307**, 341 (2016).
- [15] T. N. Szegedi *et al.* (unpublished).
- [16] D. De Frenne, *Nucl. Data. Sheets* **110**, 2081 (2009).
- [17] N. A. Roughton, M. R. Fritts, R. J. Peterson, C. S. Zaidins, and C. J. Hansen, *At. Data Nucl. Data Tables* **23**, 177 (1979).
- [18] W. R. Leo, *Techniques for Nuclear and Particle Physics Experiments* (Springer-Verlag, Berlin, 1992).
- [19] T. Szücs, G. G. Kiss, G. Gyürky, Z. Halász, Z. Fülöp, and T. Rauscher, *Phys. Lett. B* **776**, 396 (2018).
- [20] J. F. Ziegler, M. D. Ziegler, J. P. Biersack, Code SRIM, Version 2008.4, available online: <http://www.srim.org/SRIM/SRIMLEGL.htm>
- [21] R. A. Esterlund and B. D. Pate, *Nucl. Phys.* **69**, 401 (1965).
- [22] H. P. Graf and H. Münzel, *J. Inorg. Nucl. Chem.* **36**, 3647 (1974).
- [23] G. G. Kiss, T. N. Szegedi, P. Mohr, M. Jacobi, Gy. Gyürky, R. Huszánk, and A. Arcones, *Astroph. J.* **908**, 202 (2021).
- [24] T. Rauscher and F.-K. Thielemann, *At. Data Nucl. Data Tables* **75**, 1 (2000).
- [25] T. Rauscher, *Int. J. Mod. Phys. E* **20**, 1071 (2011).
- [26] A. J. Koning, S. Hilaire, and M. C. Duijvestijn, computer code TALYS, in *Proceedings of the International Conference on Nuclear Data for Science and Technology*, April 22–27, 2007, Nice, France, edited by O. Bersillon, F. Gunsing, E. Bauge, R. Jacqmin, and S. Leray (EDP Sciences, Les Ulis, 2008), pp. 211–214; available online: <http://www.talys.eu/>.
- [27] S. Watanabe, *Nucl. Phys.* **8**, 484 (1958).
- [28] L. McFadden and G. R. Satchler, *Nucl. Phys.* **84**, 177 (1966).
- [29] P. Demetriou *et al.*, *Nucl. Phys. A* **707**, 253 (2002).
- [30] V. Avrigeanu, M. Avrigeanu, and C. Manaiescu, *Phys. Rev. C* **90**, 044612 (2014).
- [31] P. Mohr, Z. Fülöp, G. Gyürky, G. G. Kiss, and T. Szücs, *Phys. Rev. Lett.* **124**, 252701 (2020).
- [32] P. Mohr, G. G. Kiss, Z. Fülöp, D. Galaviz, G. Gyürky, and E. Somorjai, *At. Data Nucl. Data Tables* **99**, 651 (2013).
- [33] C. Winteler *et al.*, *Astrophys. J.* **750**, L22 (2012).
- [34] Reaction rate database REACLIB, version 2.0, <https://groups.nslc.msu.edu/jina/reactlib/db/>
- [35] R. H. Cyburt, A. M. Amthor, R. Ferguson, Z. Meisel, K. Smith, S. Warren, A. Heger, R. D. Hoffman, T. Rauscher *et al.*, *Astroph. J. Suppl.* **189**, 240 (2010).
- [36] J. Bliss, M. Witt, A. Arcones, F. Montes, and J. Pereira, *Astrophys. J.* **855**, 135 (2018).